# Toward the Assimilation of the Atmospheric Surface Layer Using Numerical Weather Prediction and Radar Clutter Observations

ALI KARIMIAN AND CAGLAR YARDIM

*Scripps Institution of Oceanography, University of California, San Diego, La Jolla, California*

TRACY HAACK

*Naval Research Laboratory, Monterey, California*

PETER GERSTOFT AND WILLIAM S. HODGKISS

*Scripps Institution of Oceanography, University of California, San Diego, La Jolla, California*

TED ROGERS

*Atmospheric Propagation Branch, Space and Naval Warfare Systems Center, San Diego, California*

(Manuscript received 29 November 2012, in final form 21 May 2013)

ABSTRACT

Radio wave propagation on low-altitude paths over the ocean above 2 GHz is significantly affected by negative refractivity gradients in the atmospheric surface layer, which form what is often referred to as an evaporation duct (ED). Refractivity from clutter (RFC) is an inversion approach for the estimation of the refractivity profile from radar clutter, and RFC-ED refers to its implementation for the case of evaporation ducts. An approach for fusing RFC-ED output with evaporation duct characterization that is based on ensemble forecasts from a numerical weather prediction (NWP) model is examined here. Three conditions of air–sea temperature difference (ASTD) are examined. Synthetic radar clutter observations are generated using the Advanced Propagation Model. The impacts of ASTD on the evaporation duct refractivity profile, atmospheric parameter inversion, and propagation factor distributions are studied. Relative humidity at a reference height and ASTD are identified as state variables. Probability densities from NWP ensembles, RFC-ED, and joint inversions are compared. It is demonstrated that characterization of the near-surface atmosphere by combining RFC-ED and NWP reduces the estimation uncertainty of ASTD and relative humidity in an evaporation duct, with respect to using either method alone.

## 1. Introduction

Knowledge of the atmospheric surface layer (ASL) is crucial in weather prediction and in the prediction of radar and communication systems performance at frequencies above 2 GHz on low-altitude paths. Bulk measurements and rocketsondes are in situ methods for sampling the ASL (Rowland et al. 1996). While having some limitations (Helvey 1983; Mentes and Kaymaz 2007), these methods are still in use today. Using radar clutter returns to estimate the refractivity profile in the ASL potentially can be done continuously (Rogers et al. 2000; Gerstoft et al. 2003b; Yardim et al. 2008). Shipborne radars commonly operate across the world's oceans and in many complex coastal environments. These sensors can potentially sample the ASL continuously, in otherwise data-denied regions and over water where measurements, particularly vertical profiles, are scarce.

Refractivity profiles and their corresponding radar clutter returns also can be modeled using mesoscale numerical weather prediction (NWP; Burk et al. 2003; Wang et al. 2012). Sea clutter predictions based on range-varying ASL characterization from the Coupled Ocean–Atmosphere Mesoscale Prediction System (COAMPS) (Hodur 1997) were shown by Burk et al. (2003) to be in agreement with clutter observed by an S-band radar in the lee of Kauai in the Hawaiian

*Corresponding author address:* Ali Karimian, Scripps Institution of Oceanography, University of California, San Diego, 291 Rosecrans St., San Diego, CA 92106.
E-mail: alik@ucsd.edu

DOI: 10.1175/JAMC-D-12-0320.1

Islands. Mesoscale NWP has steadily improved over time and good levels of agreement with observed ASL values have been reported (Haack et al. 2010; Wang et al. 2012).

Mesoscale NWP models cannot represent all processes in the atmosphere, and there always is some degree of error in the information that is assimilated into the model. The uncertainty of the estimations increases as the distance (in both space and time) increases from the observations that have been assimilated. The spatial resolution of the NWP also might be too coarse to capture vertical variations of the atmosphere (Warner 2011).

Refractivity-from-clutter (RFC) techniques use observed radar backscatter to estimate the ambient environment refractivity profile (Karimian et al. 2011; Zhao and Huang 2012). A strong correlation between the retrieved refractivity profile using an S-band radar and in situ measurements by instrumented aircrafts has been noted (Rogers et al. 2000; Gerstoft et al. 2003b). RFC techniques enable the tracking of spatial and temporal changes in the environment (Vasudevan et al. 2007; Yardim et al. 2008). There have been attempts to incorporate the worldwide surface meteorological observations database using the environmental library of the Advanced Refractive Effects Prediction System (Patterson 1998) in the RFC inversion (Yardim et al. 2009). This method uses regional meteorological duct height statistics as a prior probability density in refractivity profile inversions.

One drawback of RFC is the increased variance in the estimated refractivity above the atmospheric duct (Yardim et al. 2007). NWP potentially can be used to regularize the RFC-ED solution above the duct. On the other hand, RFC inversions potentially can reduce the NWP errors by increasing the number of observations from RFC-capable ships. Here, the application of RFC in evaporation ducting conditions is referred to as RFC-ED.

The COAMPS model is used here to generate ensembles of air and sea temperatures, relative humidity, and wind predictions at 10 m above the sea. These ensembles are converted to vertical atmospheric profiles in the vicinity of the sea surface using the Navy Atmospheric Vertical Surface Layer Model (NAVSLaM; Frederickson 2010). The atmospheric profile obtained from the previous step is used in a joint cost function minimization framework together with observed clutter power to invert for the air-sea temperature difference (ASTD) and the relative humidity in the ASL. It is shown that the uncertainty of the estimated atmospheric variables is reduced within this joint framework compared to using either NWP or RFC-ED alone. Subsequently, estimated atmospheric parameter probability distributions are used to obtain the radio refractivity profile distribution, which in turn is used to find the distribution of the propagation factor for electromagnetic waves. The latter is important in the analysis of radio wave propagations and the assessment of radar coverage in an environment (Yardim et al. 2009).

The dependence of the environmental refractivity index on the atmospheric parameters is discussed in section 2, with an emphasis on evaporation ducting conditions. Inversions of the refractivity profile and atmospheric bulk parameters using radar clutter observations are discussed in section 3. Mesoscale NWP and ensemble methods are reviewed in section 4. Integration of NWP and RFC-ED for inversion of the atmospheric bulk parameters, and subsequently the derivation of the probability distribution of the propagation factor, are discussed in section 5.

## 2. Dependence of refractivity index on atmospheric parameters

Humidity typically decreases rapidly in the ASL above the ocean surface, resulting in a leaky waveguide that bends radio waves toward the surface. This feature is known as an evaporation duct. Maritime evaporation ducts are almost always present around the globe (Skolnik 2008) and usually affect both low-altitude radar detection and maximum communication ranges. As a consequence, correct characterization of the ASL is important in determining the performance of these systems.

The vertical modified refractivity $M$ is defined as the part per million deviation of the index of refraction $n$ from that of a vacuum after transforming the spherical earth propagation into a flat earth problem. The modified refractivity $M$ is a function of atmospheric variables with experimental constants for frequencies 0.1–100 GHz (Thayer 1974; Bevis et al. 1994):

$$M(z)=\frac{77.6P(z)}{T_{\text{air}}(z)}-\frac{5.6e(z)}{T_{\text{air}}(z)}+3.75\times10^{5}\frac{e(z)}{T_{\text{air}}^{2}(z)}+0.1568z, \tag{1}$$

where $P(z)$ and $e(z)$ are the atmospheric pressure and partial pressure of water vapor (hPa) and $T_{\text{air}}(z)$ is the absolute air temperature (K), all at altitude $z$ (m). Monin–Obukhov (MO) similarity theory is widely accepted as the means to relate physical quantities and processes in the ASL (Foken 2006). MO-based models can generate vertical atmospheric profiles given the sea surface temperature $T_{\text{sea}}$, and values at a reference height of air temperature, wind speed $u$, and relative humidity (RH). Corresponding vertical refractivity profiles can subsequently be obtained using (1). Except for

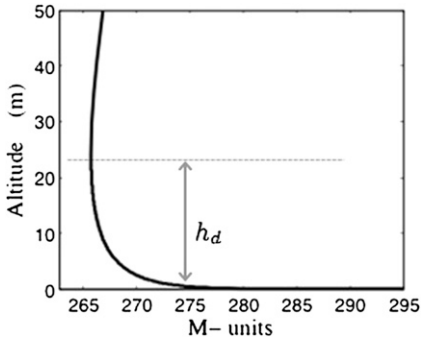


FIG. 1. The modified refractivity profile of an arbitrary evaporation duct with $\Delta T = 0$ and duct height $h_d = 24$ m.

relatively rare subrefractive cases, the vertical $M(z)$ profile is concave with respect to height $z$ and has an inflection point referred to as the evaporation duct height $h_d$, as illustrated in Fig. 1. As a point of clarification, the vertical $M$ profile is not uniquely defined by $h_d$ in most MO models including those of Liu et al. (1979) and Frederickson et al. (2000).

Several MO evaporation duct models exists (Cook and Burk 1992; Babin et al. 1997; Frederickson et al. 2000; Frederickson 2010). We choose NAVSLaM (Frederickson et al. 2000; Frederickson 2010) to compute the vertical atmospheric and refractivity profiles in an evaporation duct from bulk parameters (air temperature, humidity, and pressure at a certain height above the sea surface). Bulk parameters can be provided by in situ measurements, climatological databases, or NWP. NAVSLaM uses an iterative method. The evaporation duct height is much more sensitive to variations in NAVSLaM model parameters in stable conditions, which results in increased profile errors. Especially in highly stable thermal stratification and low winds, the algorithm either fails to converge or provides highly erroneous $M$ profiles. However, there are built-in safety loops in the code, such as when the results are rejected if the process takes more than a certain number of iterations. Some of the problems with evaporation duct height estimation under stable conditions are discussed in detail in Babin et al. (1997). An alternative to NAVSLaM could be using a noniterative method to find the evaporation duct height (Babin and Dockery 2002).

Changes in duct height versus ASTD ($\Delta T = T_{\text{air}} - T_{\text{sea}}$), relative humidity, and wind speed are shown in Fig. 2 for sea temperatures $T_{\text{sea}} = 15°$ and 30°C. Atmospheric variables $T_{\text{air}}$, RH, and $u$ are all taken at 10 m. In general, ASL models are insensitive to the atmospheric pressure (Fairall et al. 2003), and a typical atmospheric pressure of 1020 hPa is used here. Figure 2 shows rapid changes to the duct height with $\Delta T$ where $\Delta T > 0$, and fewer variations where $\Delta T < 0$. Comparison of Figs. 2a,c and 2b,d shows

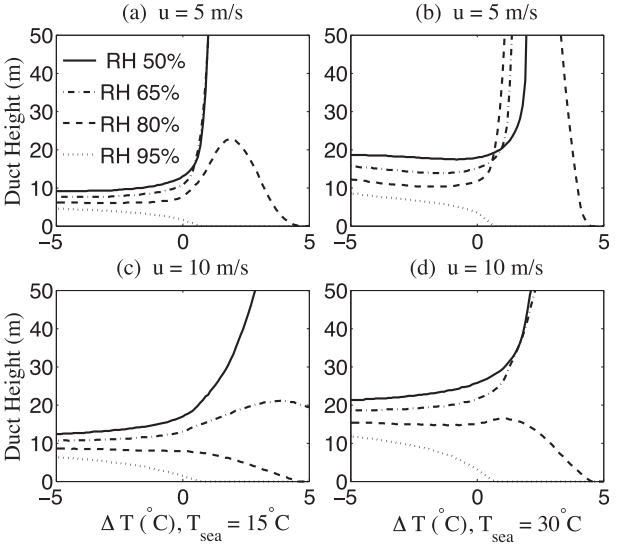


FIG. 2. Evaporation duct height vs $\Delta T = T_{\text{air}} - T_{\text{sea}}$ and RH for wind speed $u$ of (a),(b) 5 and (c),(d) 10 m s$^{-1}$ obtained by NAVSLaM and $T_{\text{sea}}$ = (left) 15° and (right) 30°C. All atmospheric variables are referenced to 10 m above the sea surface.

that the sensitivity of duct height to $\Delta T$ and RH in warm sea waters is more significant than in colder waters. Clearly, the sensitivity of $h_d$ to changes in $\Delta T$, RH, and $u$ is state dependent, and small errors in $\Delta T$, RH, and $u$ can result in large errors in $h_d$ when $\Delta T > 0$.

## 3. Refractivity from clutter

Radar clutter in a maritime environment depends on the two-way propagation loss from the transmitter to the range cell, and propagation loss depends on the refractivity profile. Assume an environment described by a vector of model parameters **m** through which the electromagnetic waves are propagated. Previous RFC-ED studies have considered the duct height of an evaporation duct as the state parameter (Rogers et al. 2000; Yardim et al. 2009; Douvenot et al. 2010) under the assumption that $\Delta T = 0$. This assumption was important to constrain the possible atmospheric solutions. The vector of atmospheric parameters $\mathbf{m} = [\Delta T, \text{RH}]^{\text{T}}$ at a height of 10 m is used here as the state vector.

### a. Sea clutter model

The expected radar clutter power in a maritime environment can be expressed as a function of the radar parameters; the propagation factor $F$, which is a function of the refractivity profile **m** and range $r$; and the grazing angle $\theta$ (Skolnik 2008):

$$P_c(\mathbf{m}, r) = \frac{P_t G^2 \lambda^2 \theta_B c\tau \sigma_0 \sec(\theta) F^4(\mathbf{m}, r)}{2(4\pi r)^3 L}, \qquad (2)$$

where $P_t$ is the transmitter power, $G$ is the antenna gain, $\lambda$ is the wavelength, $\theta_B$ is the antenna pattern azimuthal beamwidth, $c$ is the propagation speed, $\tau$ is the pulse width, $\sigma_0$ is the expected sea surface reflectivity per unit area, and $L$ is the total assumed system losses. The grazing angle $\theta$ is the angle between the incident ray and the sea surface and it is a function of $\mathbf{m}$ and $r$. The sea surface reflectivity in ducting conditions typically is computed based on the work of Dockery (1990).

For simplicity, synthetic clutter powers are computed assuming range-independent refractivity profiles and wind speed, using the parabolic equation–based Advanced Propagation Model (APM) (Barrios et al. 2006). This method can easily be extended to range-dependent profiles. Clutter power is a function of grazing angle and there is a debate about the strength of this dependence, especially for very low grazing angles under ducting conditions (Gerstoft et al. 2003b; Karimian et al. 2012b). The RFC inversion algorithm can be made more robust by using clutter starting from a minimum range $r_0$ where the grazing angle converges to a constant value in an evaporation duct. It was shown in Yardim et al. (2009) that $r_0 = 5$ km is good for commonly observed evaporation ducting conditions:

$$P_{n,c}(\mathbf{m}, r) = \frac{P_c(\mathbf{m}, r)}{P_c(\mathbf{m}, r_0)} = \frac{F^4(\mathbf{m}, r) r_0^3}{F^4(\mathbf{m}, r_0) r^3}. \quad (3)$$

Letting $F$ and $P_{n,c}$ represent the associated values in decibels as opposed to real numbers, we can rewrite (3) as

$$P_{n,c}(\mathbf{m}, r) = 4[F(\mathbf{m}, r) - F(\mathbf{m}, r_0)] + 3 \log \frac{r}{r_0}. \quad (4)$$

### b. *Refractivity profile inversion and bulk parameters for evaporation ducts*

Inversion for the evaporation duct height from an S-band radar clutter was reported in Rogers et al. (2000). The sensitivity of the radar clutter power to the duct height at different frequencies was studied by Yardim et al. (2009). RFC-ED studies in the past have assumed sea and air temperatures to be equal. This assumption simplifies the refractivity profile of an evaporation duct to be logarithmic in the vicinity of the sea surface and only dependent on the duct height.

An objective function $J_{\mathrm{RFC}}$ that quantifies the difference between the normalized observed and modeled clutter power, $\mathbf{P}_{n,o}$ and $\mathbf{P}_{n,c}(\mathbf{m})$, is formed here. The $\mathbf{P}_{n,o}$ and $\mathbf{P}_{n,c}$ are the vectors of clutter power in decibels over $N$ range bins. The optimal solution minimizes the objective function:

$$\hat{\mathbf{m}} = \underset{\mathbf{m}}{\operatorname{argmin}} J_{\mathrm{RFC}}[\mathbf{P}_{n,o}, \mathbf{P}_{n,c}(\mathbf{m})]. \quad (5)$$

The backscattered radar signal can be modeled using a multiplicative random variable representing the variable sea surface reflectivity and additive thermal noise. Following Skolnik (2008), variation of the sea surface reflectivity is assumed to have a lognormal density. Working in the high clutter-to-noise ratio (CNR) regime, the additive noise term can be neglected. Therefore, the observed clutter power in the logarithmic domain is obtained as

$$\mathbf{P}_{n,o} = \mathbf{P}_{n,c}(\mathbf{m}) + \mathbf{n} \quad \text{and} \quad (6)$$

$$\mathbf{n} \sim \mathcal{G}(0, \mathbf{C}_o), \quad (7)$$

where $\mathbf{P}_{n,o}$ and $\mathbf{P}_{n,c}(\mathbf{m})$ are in decibels, $\mathbf{n}$ is the vector of logarithmic random sea reflectivity variations that is assumed to be Gaussian, and $\mathbf{C}_o$ is the covariance matrix of sea surface reflectivity variations. The log-likelihood objective function $J_{\mathrm{RFC}}$ is expressed by

$$J_{\mathrm{RFC}} = [\mathbf{P}_{n,o} - \mathbf{P}_{n,c}(\mathbf{m})]^{\mathrm{T}} \mathbf{C}_o^{-1} [\mathbf{P}_{n,o} - \mathbf{P}_{n,c}(\mathbf{m})]. \quad (8)$$

The slow rate of change of the clutter power with range at the frequencies of interest enables the selection of RFC range bin widths on the order of hundreds of meters without any loss of clutter features. In addition, large bin widths justify the assumption that the modeled sea surface variations at consecutive bins are independent. Thus, $\mathbf{C}_o = \nu \mathbf{I}$, where $\nu$ is the variance of the logarithmic sea surface reflectivity and $\mathbf{I}$ is the identity matrix. Equation (8) is the negative log-likelihood function under lognormal radar cross-sectional statistics. Modeling random variations of the clutter power due to the changes in the sea surface reflectivity by the lognormal density often is a good approximation in RFC applications (Karimian et al. 2012a).

A weakness of RFC-ED as a stand-alone means for characterizing the ASL's refractivity is in using a log-linear refractivity profile defined by a single parameter (Rogers et al. 2000). This simplification causes small errors when the inverted refractivity profile obtained from RFC-ED is used for propagation calculations at the same frequency as the sensing radar. Errors increase, though, as the difference between the frequencies of the sensing and the use of the profiles increases. Figure 3 shows that not only the duct height, but also the shape of the profile, affects the radar clutter. This effect is more pronounced at higher frequencies. In this example, the sea surface temperature is 30°C, wind speed is 5 m s$^{-1}$, and radar is 10 m above the sea surface. The clutter

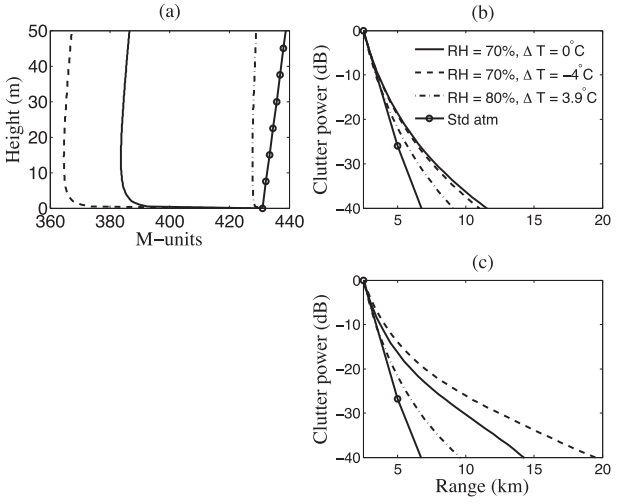


FIG. 3. (a) Modified refractivity profiles, all with duct heights of 14 m. Also shown are the corresponding clutter powers when the radar is located at 10 m for operational frequencies of (b) 3 and (c) 10 GHz. The $T_{sea} = 30°C$ and $u = 5\,m\,s^{-1}$.

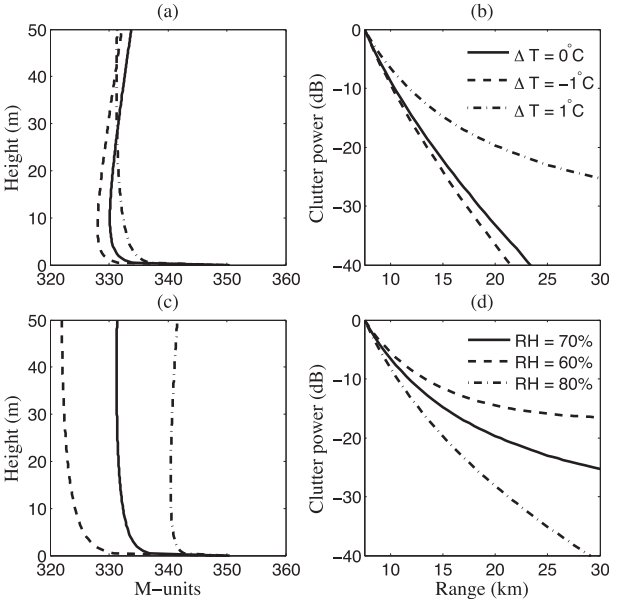


FIG. 4. (a),(c) Modified refractivity profiles and (b),(d) the corresponding clutter powers. Radar frequency is 3 GHz, and it is located at 10 m above the sea surface. The $T_{sea} = 15°C$ and $u = 5\,m\,s^{-1}$. In (a) and (b), RH = 70% for different $\Delta T$ conditions; in (c) and (d), $\Delta T = 1°C$ for different humidities.

power fall-off rates for a 14-m duct in $\Delta T < 0$ and $\Delta T = 0$ conditions are similar at 3 GHz. However, those fall-off rates differ at 10 GHz. Thus, knowledge of the bulk parameters is required when inverted parameters at one frequency are to be used at a different frequency. Using the refractivity profile obtained from NWP might improve the modeling error at other frequencies. Figures 3 and 4 both use NAVSLaM to obtain the refractivity profile from COAMPS parameters. APM (Barrios et al. 2006) then is used to compute the clutter power from these refractivity profiles.

The radar clutter power is sensitive to changes in the atmospheric variables. Dodgett (1997) showed that radar propagation is also more sensitive to changes in humidity and temperature than to those in pressure levels. Figure 4 demonstrates the sensitivity of the clutter power to atmospheric parameters. Figure 4 also shows the changes in the clutter power of a radar at 10 m above the sea surface, operating at 3 GHz, when ASTD changes by 1°C, or relative humidity changes by 10%. Here, it is assumed that pressure is constant; surface temperature and wind speed are obtained from COAMPS ensemble forecasts; and radar clutter is used to invert for humidity and ASTD.

## 4. Numerical weather prediction

COAMPS is a nonhydrostatic mesoscale model developed from the Navier–Stokes equations that produces predictions of the ocean and atmosphere on time scales of hours to several days (Hodur 1997). This model can be used for the prediction of winds, potential temperature, perturbation pressure, and five species of water and their autoconversions including mixing ratios of water vapor, clouds, rain, snow, ice, and graupel. It contains physical parameterizations appropriate for high-resolution characterizations of the surface energy budget, surface fluxes, planetary and marine boundary layers, short- and longwave radiation, and convection.

External sources of data such as measurements from radiosondes and aircraft, buoy, and ship data can be used to blend the observed data with the first-guess field generated by COAMPS (Hodur et al. 2001). Multivariate optimum interpolation analysis of wind and pressure and univariate interpolation of temperature and moisture are used to combine the observational data with the first guess from the COAMPS previous 12-h forecast.

Three nested grids were used here in forecasts with horizontal spacings of 45, 15, and 5 km, respectively. Each domain has 45 vertical levels with the lowest located at 10 m. The vertex of the grid with 5-km resolution (origin in Figs. 5 and 6) is at 18.10048°N, 199.0548°E, southwest of the Hawaiian Islands. Sea temperatures are obtained from satellite data, and no perturbation is introduced to this parameter in the generation of ensemble members. Here, the ensemble transform (Bishop and Toth 1999) is used to generate initial states for ensemble predictions (McLay et al. 2008). One of the

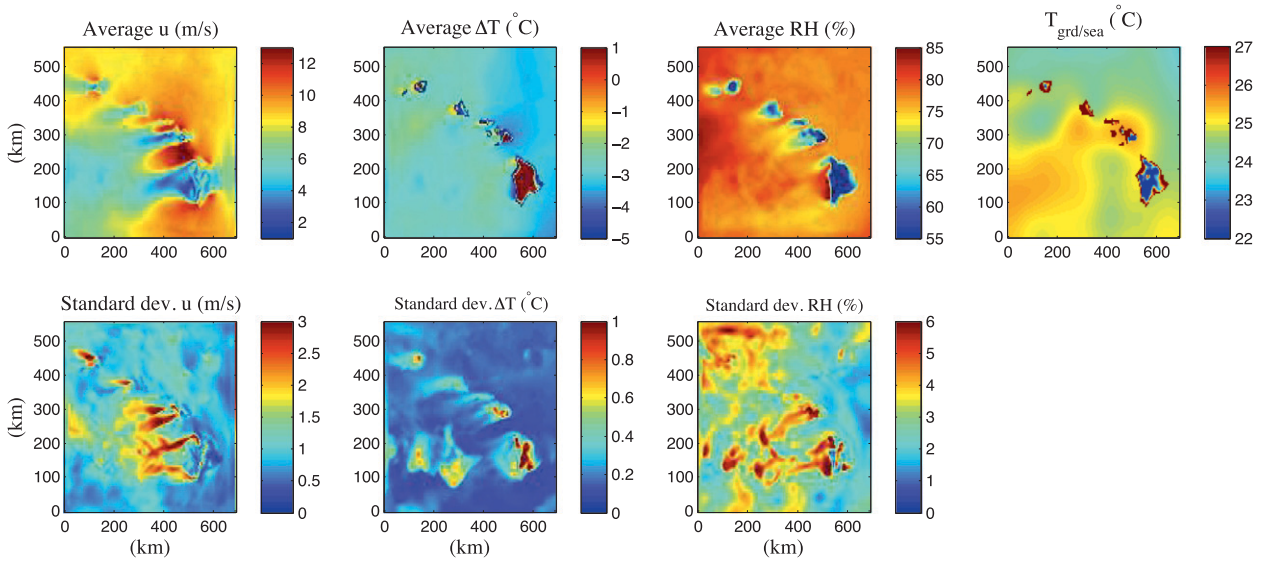


FIG. 5. (top) Average values and (bottom) standard deviation of COAMPS ensemble of (left) wind speed, (left center) $\Delta T$, and (right center) RH at 10 m around the Hawaiian Islands at 1200 UTC 7 May 2008 using 5-km grid spacings. (right) The observed surface temperature (sea or ground) during the same time using buoy and ship data.

ensemble members is the control run and the rest are run with perturbed conditions. The error covariance of the ensemble with respect to the average prediction is formed at the start of each forecast cycle (i.e., every 6 h).

Two NWP ensembles in the region of the Hawaiian Islands are used here that are known to have evaporation ducting conditions. The first is a 16-member ensemble on the air–sea boundary layer at 1200 UTC 7 May 2008, and the second is a 32-member ensemble that corresponds to 26–28 July 2008 with 3-h gaps starting from 1200 UTC. The data that correspond to 1200 UTC 7 May 2008 are shown in Fig. 5. Atmospheric parameters shown in Fig. 5 are all at 10 m. Sea temperature in general is higher than the air temperature in this dataset. COAMPS outputs at 10 m are used as inputs to NAVSLaM to find the evaporation duct profiles at each location. The average and standard deviation of duct heights are shown in Fig. 6. Duct height is not very sensitive to $\Delta T$ changes where the air temperature is less than the sea temperature. The ensemble for 26–28 July 2008 shows similar variations in the standard deviation of the atmospheric variables and duct heights, which are not shown.

Ensemble methods provide the environmental parameter uncertainty in NWP predictions. This will allow the integration of the NWP results with the RFC. The data assimilation method given in the next section will merge these two sources of information (NWP and RFC) onto the ASL parameters, taking into account how much confidence we have in each method via the uncertainties attached to each method.

## 5. Integration of radar observations and weather prediction

Data assimilation generally can be described as an optimization problem to integrate observations with predictions (Kalnay 2003). Gerstoft et al. (2003a) used clutter powers from multiple grazing angles to infer the refractivity profile of surface ducts and introduced limits on possible refractivity profile solutions from climatological constraints. Within a similar framework, ocean salinity and temperature measurements in the water column were used to update the water-mass properties in oceanic circulation models (Thacker and Esenkov 2002). Underwater acoustic propagation loss has been used by Lermusiaux et al. (2011) for coupled oceanographic and acoustic data assimilation.

A quadratic metric is defined to measure the fitness of each set of candidate atmospheric variables ($\mathbf{m}$) to predicted values by NWP and inversions of observed clutter power $\mathbf{P}_o$. Here, $\mathbf{m} = [\Delta T, \mathrm{RH}]^{\mathrm{T}}$, with atmospheric variables at a height of 10 m. The clutter power fall-off rate does not convey information about the air pressure and the absolute value of the wind speed, and it is a weak function of sea surface temperature. Hence, these are used directly from NWP.

Variational data assimilation studies typically have considered a quadratic cost function that assumes the prediction and observation error terms to have Gaussian densities (Kalnay 2003; Warner 2011). The joint cost function of NWP and RFC-ED is obtained by statistics yielded from the NWP ensemble and the RFC-ED inversion Eq. (8):

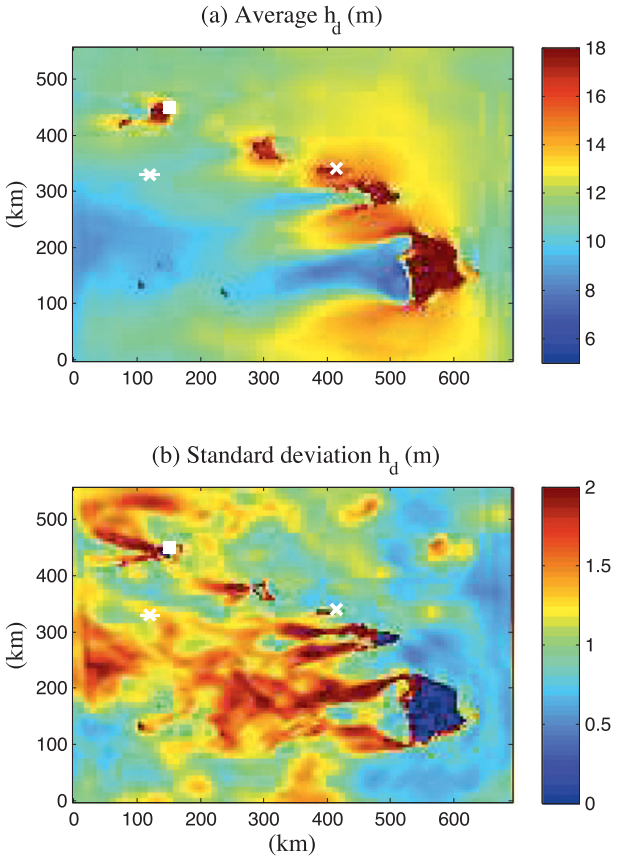


FIG. 6. (a) Average and (b) standard deviation of duct heights obtained by running NAVSLaM on the COAMPS ensemble in Fig. 5. The geographic locations of cases analyzed in Figs. 7, 8, and 9 are marked by white asterisks, times signs, and squares, respectively.

$$J(\mathbf{m}) = J_{\mathrm{NWP}}(\mathbf{m}) + J_{\mathrm{RFC}}(\mathbf{m}) = \frac{1}{2}(\mathbf{m}-\boldsymbol{\mu}_{\mathrm{NWP}})^{\mathrm{T}}\mathbf{C}_N^{-1}(\mathbf{m}-\boldsymbol{\mu}_{\mathrm{NWP}}) + \frac{\lambda}{2}[\mathbf{P}_{n,o}-\mathbf{P}_{n,c}(\mathbf{m})]^{\mathrm{T}}\mathbf{C}_o^{-1}[\mathbf{P}_{n,o}-\mathbf{P}_{n,c}(\mathbf{m})], \quad (9)$$

where $\boldsymbol{\mu}_{\mathrm{NWP}}$ and $\mathbf{C}_N$ are the average and covariance of NWP ensemble atmospheric variables. Ensemble members are assumed to be independently and identically distributed samples in the RH–$\Delta T$ space. Hence, the covariance matrix can be approximated with the sample covariance. The larger the number of ensemble members, the better the estimate is going to be. Even though the available dataset had a 16-element ensemble for one of the examples, future implementations will be using a minimum of 32 ensemble members. The $\lambda$ is a constant to balance the effect of RFC-ED and NWP on the joint penalty function. Here, $\lambda = 1$ is used, which corresponds to a Bayesian solution using the NWP term as a prior and

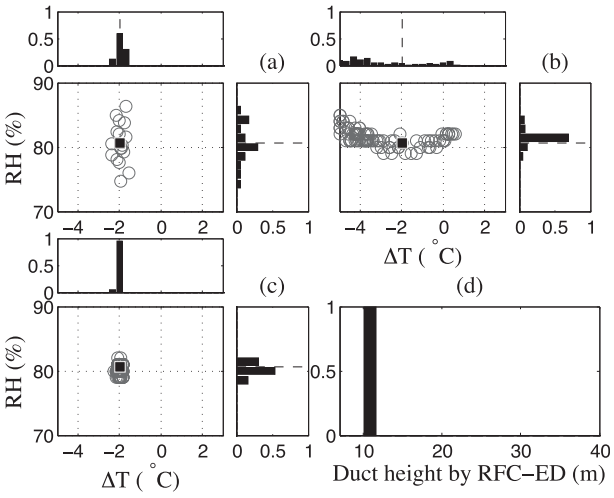


FIG. 7. Case 1, $\Delta T < 0$ corresponding to 1200 UTC 7 May 2008 at position (120, 330) km in Figs. 5a–c. Scatterplots of $\Delta T$ and RH, and each of their marginal densities obtained by (a) the COAMPS ensemble, (b) RFC-ED, and (c) the joint NWP–RFC-ED method. The NWP ensemble mean (squares) is used for clutter power simulations. (d) Histogram of duct heights obtained by RFC-ED in (b).

RFC-ED as the likelihood term with Gaussian variations. A two-dimensional search through the $\Delta T$ and RH parameter space is used here to find the optimum $\mathbf{m}$.

Analysis of NWP outputs indicates that assuming a range-independent profile for a radius of 20–25 km is reasonable far from the coasts. Simulations in this paper are made by taking the average COAMPS predictions at the location of interest and assuming that the $\Delta T$, humidity, and wind profiles are range independent up to a range of 25 km. The same approach can be extended to range-dependent profile inversions where the state vector will be larger.

Three atmospheric conditions classified by values of $\Delta$T are investigated. The cases of $\Delta T > 0$, $\Delta T = 0$, and $\Delta T < 0$ loosely correspond to the stable, neutral, and unstable thermodynamic atmospheric conditions, respectively. The geographic locations of these examples are shown with white crosses in Fig. 6. The most prevalent situation in the dataset is the $\Delta T < 0$ condition. This condition is investigated with the example in Fig. 7. The $\Delta T = 0$ condition occurs rarely. One example of this condition is studied in Fig. 8. The $\Delta T > 0$ condition in our dataset occurs only near the coast where the assumption of a range-independent profile fails. We only use the range-independent refractivity profile assumption in Fig. 9 to demonstrate an inversion example under the $\Delta T > 0$ condition. The priors for $\Delta T$ and RH for RFC-ED inversions are assumed to be uniformly distributed with $\Delta T = (-4°, 2°\mathrm{C})$ and RH = (50%, 100%) for all examples.

All three examples in Figs. 7–9 consider the radar clutter with CNR of 25 dB at the range of 10 km. A 5°

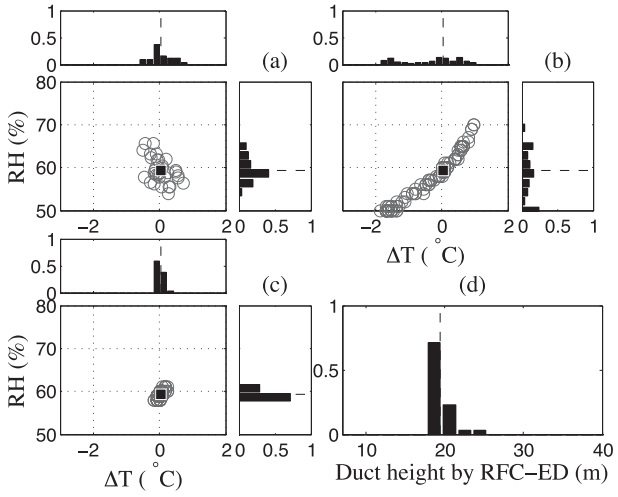


FIG. 8. As in Fig. 7, but for case 2, $\Delta T = 0$ corresponding to 0300 UTC 27 Jul 2008 at position (415, 340) km.

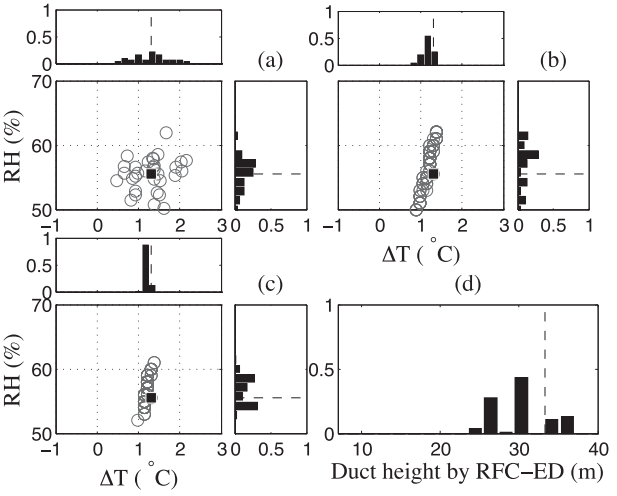


FIG. 9. As in Fig. 7, but for case 3, $\Delta T > 0$ corresponding to 1200 UTC 28 Jul 2008 at position (150, 450) km.

azimuthal segment is used for each inversion where synthetic clutter power is generated with independent noises and 1° azimuthal spacing. The logarithmic radar cross section is assumed to have a Gaussian density with 0 mean and 3-dB standard deviation. The average of the NWP ensemble is taken as the true state and used to generate 100 clutter power realizations. Synthetic clutter powers in the range of 5–25 km with bins every 1 km are used for RFC-ED inversions and joint NWP–RFC-ED inversions. Implementation of RFC-ED is based on the minimization of (8), and implementation of joint NWP-RFC-ED is based on using the cost function (9). Two-dimensional and marginal densities of the NWP ensemble, RFC-ED inversions, and joint inversions are all demonstrated in these plots. Histograms of inverted duct heights obtained from RFC-ED inversions are also plotted.

An example with $\Delta T < 0$ corresponding to 1200 UTC 7 May 2008 at position (120, 330) km in Fig. 5 is shown in Fig. 7. RFC-ED is insensitive to $\Delta T$ and more sensitive to the humidity. This is consistent with Fig. 2, where the duct height is rather insensitive to $\Delta T$ where $\Delta T < 0$ but is highly sensitive to changes in the level of relative humidity. In contrast, the NWP has a larger uncertainty for RH and smaller for $\Delta T$. Hence, the combination of RFC-ED and NWP reduces the uncertainties in atmospheric parameter estimation drastically. Figure 7a shows the distribution of a 16-member ensemble found by COAMPS. A total of 100 realizations of clutter power are obtained by adding 3-dB variance Gaussian noise to the clutter power of the average ensemble. Inversion results of these clutter power realizations are shown in Fig. 7b. The distribution of pairs of $[\Delta T, \mathrm{RH}]^{\mathrm{T}}$ found by RFC-ED form a curve of points with very similar duct heights. This is shown by the narrow histogram of inverted duct heights in Fig. 7d. This is consistent with strong dependence of clutter power on duct height, especially with $\Delta T \leq 0$ (Rogers et al. 2000). Figure 7c shows the distribution of atmospheric parameters using minimization of the joint cost function (9).

An example with almost $\Delta T = 0$ is considered in Fig. 8. Figure 8a shows the distribution of the atmospheric parameters obtained from 32 COAMPS ensemble predictions. RFC-ED, shown in Fig. 8b, provides a set of solutions that all correspond to similar clutter power patterns. These solutions all yield similar duct heights, as demonstrated by the narrow probability density in Fig. 8d. Similarity of duct heights of inverted profiles is expected, since clutter power is a strong function of the duct height in evaporation ducts, rather than the minor changes in the refractivity index gradient. The joint inversion of NWP and RFC-ED, shown in Fig. 8d, reduces the uncertainty of the lower-atmospheric parameter estimation found from either method.

An example with $\Delta T > 0$ is demonstrated in Fig. 9. Figure 9a shows the distribution of 32 ensemble predictions of COAMPS. Figure 9b shows inversion results of 100 clutter power realizations, obtained by adding 3-dB variance Gaussian variations on the clutter power of the average ensemble. The duct-height uncertainty obtained from RFC-ED (Fig. 9d) is increased in this case ($\Delta T > 0$) compared to other cases seen in two previous examples. The reason is that the $M$ profile converges to a vertical profile when $\Delta T > 0$. For example, compare the shape of the $M$ profiles in Fig. 3, where all $M$ profiles have the same duct height.

The environment can evolve after earlier COAMPS predictions. An example of this scenario is provided in

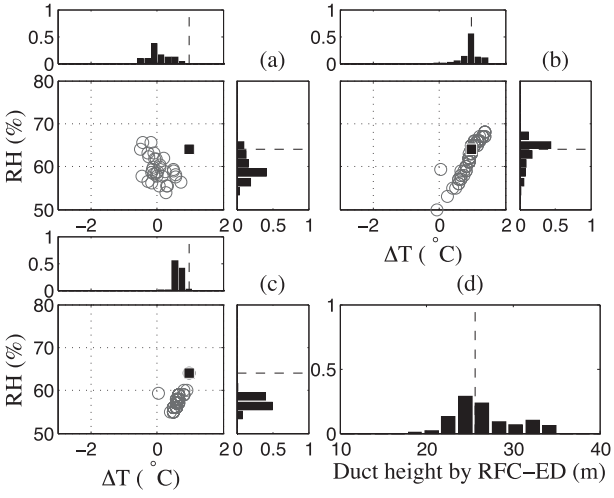


FIG. 10. As in Fig. 7, but for case 4, evolution of the environment after predictions. The scatterplot of $\Delta T$ and RH, and their marginal densities are obtained in (a) by COAMPS from Fig. 8. The square shows the assumed true state used for clutter power simulations.

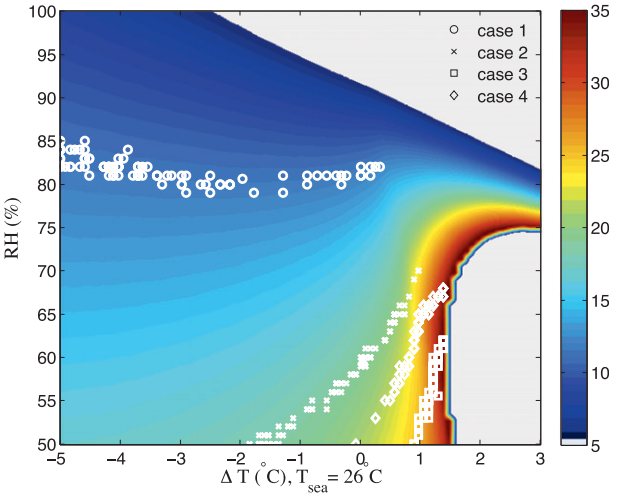


FIG. 11. Duct height (circles) (m) as a function of $\Delta T$ and RH with $T_{sea} = 26°C$ and $u = 8\,m\,s^{-1}$, conditions similar to those of the average ensemble in Fig. 5. Symbols with legend at top right show inversion results obtained by RFC-ED with cases 1–4 referring to Figs. 7–10, respectively.

Fig. 10. This example considers the original atmospheric parameters to be $\Delta T = 0$ and RH = 60% obtained by COAMPS. The environment is assumed to have evolved into a new state where $\Delta T = 1.5°C$ and RH = 65%. The combination of RFC-ED and NWP helps to obtain inversion results closer to the current environmental state.

Constant duct-height contours are shown in Fig. 11, with conditions similar to Figs. 7–10. Inverted atmospheric parameters obtained from RFC-ED in those examples also are shown. The inversion results follow the contours of the duct height (as seen in Fig. 11) due to the strong dependence of the clutter power on duct height. This is consistent with narrow histograms of duct heights obtained from RFC-ED inversions in panel d of Figs. 7–10. This shows that in most cases RFC can invert for the duct height accurately but that does not translate into a unique solution in the atmospheric parameter domain. This creates RFC uncertainty surfaces that closely follow the constant duct-height contours. NAVSLaM does not provide reliable refractivity profiles for large positive $\Delta T$ (white area in Fig. 11). Thus, the spread of inverted duct-height histograms gets larger for $\Delta T > 0$. Subsequently, inverted duct heights obtained from RFC-ED diverge from contours with larger positive $\Delta$T in Fig. 11.

The propagation factor $F$ is defined as the ratio of the magnitude of the electric field at a given point under specified conditions to the magnitude of the electric field under free-space conditions with the same transmitter: $F(r) = |E(r)/E_{fs}(r)|$ (Skolnik 2008). The probability densities of the propagation factor using atmospheric parameters from the three methods discussed are shown in Fig. 12 for heights of 10 and 40 m and a range of 25 km. This example uses 1000 synthetic clutter powers in each case to generate histograms. The propagation factor probability density obtained from NWP appears to have a flat distribution and is more peaked for RFC-ED. RFC-ED yields atmospheric parameters that result in similar clutter power and, thus, also result in similar propagation factors. The probability density of $F$ using the joint technique appears to be a combination of the propagation factor densities obtained from NWP and RFC-ED. However, this combination is not linear since the relationship between $F$ and atmospheric variables $\Delta T$ and RH is not linear. The importance of estimating the true atmospheric conditions for radar performance prediction can be seen by comparing the estimated $F$ values to the $F$ of a standard atmosphere with no ducting. Standard atmosphere propagation factors at 25-km range and heights of 10 and 40 m are −27 and −35 dB, respectively. Thus, failing to model the evaporation duct can lead to errors of 10–40 dB in the expected radar signal power in the assessment of radar propagation.

## 6. Conclusions

Numerical weather prediction and refractivity-from-clutter results were combined, opening the way for a full data assimilation of the refractivity profile. NWP and RFC can be used jointly in maritime environments to reduce the estimation variance of atmospheric variables near the sea surface. Advantages of NWP (providing prior information to a high altitude) and RFC (real-time tracking of atmospheric parameters) can be utilized jointly to provide a powerful inversion method. This

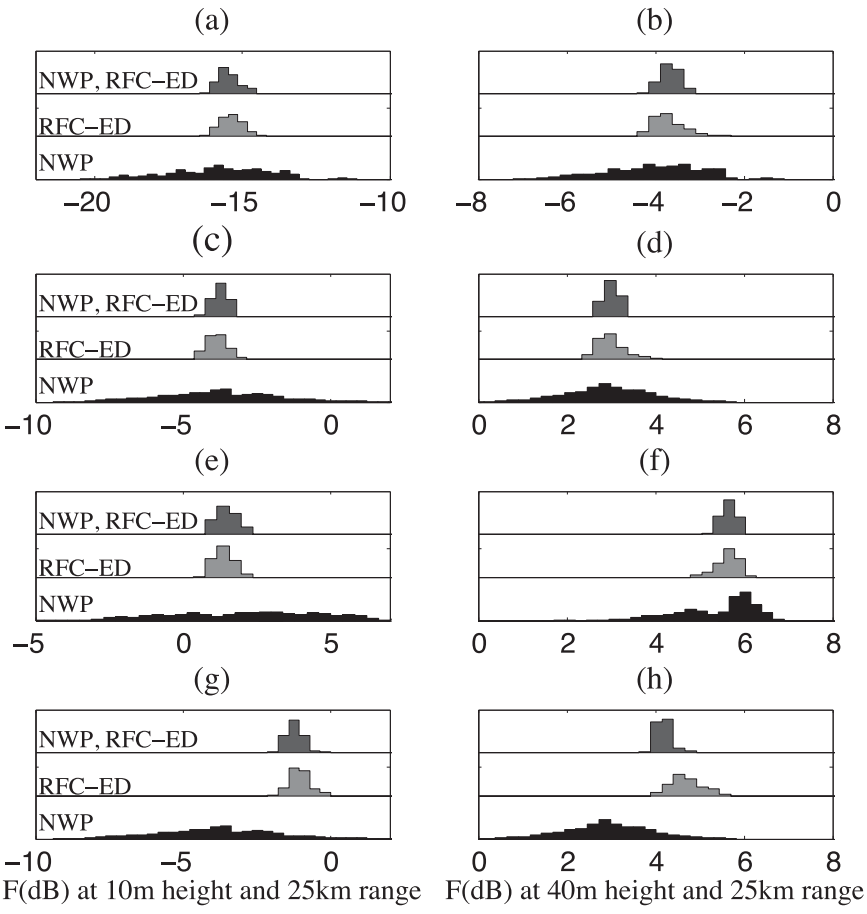


FIG. 12. The distribution of propagation factor $F$ using NWP, RFC-ED, and the joint NWP–RFC-ED method at heights of (left) 10 and (right) 40 m and a range of 25 km from an assumed source. The vertical axis is the empirical probability. (a),(b) As in Fig. 7, but with $\Delta T < 0$. (c),(d) As in Fig. 8, but with $\Delta T = 0$. (e),(f) As in Fig. 7, but with $\Delta T > 0$. (g),(h) As in the biased example in Fig. 10.

investigation focused on RFC for evaporation ducts (RFC-ED) within the atmospheric surface layer.

Spatial and temporal variabilities in the atmosphere were captured by COAMPS nonhydrostatic mesoscale forecasts at 5-km horizontal grid spacing. Atmospheric ensemble hindcasts were used here from the summer of 2008 around the Hawaiian Islands where prevailing evaporation ducting conditions were known to exist. These deterministic forecasts provided the control runs for 16- and 32-member ensemble suites. An ensemble transform technique was used in which the initial conditions at each forecast cycle were perturbed to depict how uncertainty due to errors in the initial state would evolve within the forecasts.

The RFC-ED was implemented by creating an objective function that matched the measured clutter power in a range interval and at a given azimuth to the modeled clutter power. Sea temperature, air pressure, and wind speed were directly used from NWP. Air–sea temperature difference (ASTD) and humidity were identified as the state vectors to be found by the NWP-only, RFC-ED-only, and joint methods. An ensemble of Hawaii hindcasts and a range of possible ASTD values were considered through four examples. It was shown that NWP and RFC had different sensitivities to ASTD and RH under varying stability conditions. Thus, using a joint method enabled us to reduce significantly the overall uncertainties in these parameters. Likewise, the real-time RFC updates were able to mitigate the error in atmospheric parameters created under a hypothetical case when the true environment deviated from the initial COAMPS estimates.

*Acknowledgments.* This work was supported by the Office of Naval Research under Grant N00014-13-1-0360.

## REFERENCES

Babin, S. M., and G. D. Dockery, 2002: LKB-based evaporation duct model comparison with buoy data. *J. Appl. Meteor.,* **41,** 434–446.

——, G. A. Young, and J. A. Carton, 1997: A new model of the oceanic evaporation duct. *J. Appl. Meteor.,* **36,** 193–204.

Barrios, A. E., K. Anderson, and G. Lindem, 2006: Low altitude propagation effects—A validation study of the Advanced Propagation Model (APM) for mobile radio applications. *IEEE Trans. Antennas Propag.,* **54,** 2869–2877, doi:10.1109/TAP.2006.882163.

Bevis, M., S. Businger, and S. Chiswell, 1994: GPS meteorology: Mapping zenith wet delays onto precipitable water. *J. Appl. Meteor.,* **33,** 379–386.

Bishop, C. H., and Z. Toth, 1999: Ensemble transformation and adaptive observations. *J. Atmos. Sci.,* **56,** 1748–1765.

Burk, S. D., T. Haack, L. T. Rogers, and L. J. Wagner, 2003: Island wake dynamics and wake influence on the evaporation duct and radar propagation. *J. Appl. Meteor.,* **42,** 342–367.

Cook, J., and S. Burk, 1992: Potential refractivity as a similarity variable. *Bound.-Layer Meteor.,* **58,** 151–159.

Dockery, G. D., 1990: Method for modeling sea surface clutter in complicated propagation environments. *IEE Proc. Radar Signal Process.,* **137,** 73–79.

Dodgett, M., 1997: An atmospheric sensitivity and validation study of the variable terrain radio parabolic equation model. M.S. thesis, Graduate School of Engineering, Air Force Institute of Technology, 78 pp.

Douvenot, R., V. Fabbro, P. Gerstoft, C. Bourlier, and J. Saillard, 2010: Real time refractivity from clutter using a best fit approach improved with physical information. *Radio Sci.,* **45,** RS1007, doi:10.1029/2009RS004137.

Fairall, C. W., E. F. Bradley, J. E. Hare, A. A. Grachev, and J. B. Edson, 2003: Bulk parameterization of air–sea fluxes: Updates and verification for the COARE algorithm. *J. Climate,* **16,** 571–591.

Foken, T., 2006: 50 years of the Monin–Obukhov similarity theory. *Bound.-Layer Meteor.,* **119,** 431–447.

Frederickson, P., 2010: Software design description for the Navy Atmospheric Vertical Surface Layer Model (NAVSLaM). Naval Oceanographic Office Tech. Rep. OAML-SDD-95, 35 pp.

——, K. L. Davidson, and A. K. Goroch, 2000: Operational bulk evaporation duct model for MORIAH, ver. 1.2. Naval Postgraduate School Tech. Rep. NPS/MR-2000-002, 70 pp.

Gerstoft, P., L. T. Rogers, W. S. Hodgkiss, and L. J. Wagner, 2003a: Refractivity estimation using multiple elevation angles. *IEEE J. Oceanic Eng.,* **28,** 513–525, doi:10.1109/JOE.2003.816680.

——, ——, J. L. Krolik, and W. S. Hodgkiss, 2003b: Inversion for refractivity parameters from radar sea clutter. *Radio Sci.,* **38,** 1–22, doi:10.1029/2002RS002640.

Haack, T., C. Wang, S. Garrett, A. Glazer, J. Mailhot, and R. Marshall, 2010: Mesoscale modeling of boundary layer refractivity and atmospheric ducting. *J. Appl. Meteor. Climatol.,* **49,** 2437–2457.

Helvey, R. A., 1983: Radiosonde errors and spurious surface-based ducts. *Proc. IEE F,* **130,** 643–648.

Hodur, R. M., 1997: The Naval Research Laboratory's Coupled Ocean–Atmosphere Mesoscale Prediction System (COAMPS). *Mon. Wea. Rev.,* **125,** 1414–1430.

——, X. Hong, J. D. Doyle, J. Pullen, J. Cummings, P. Martin, and M. A. Rennick, 2001: The Coupled Ocean/Atmosphere Mesoscale Prediction System (COAMPS). *Oceanography,* **15,** 88–98.

Kalnay, E., 2003: *Atmospheric Modeling, Data Assimilation, and Predictability.* Cambridge University Press, 341 pp.

Karimian, A., C. Yardim, P. Gerstoft, W. S. Hodgkiss, and A. E. Barrios, 2011: Refractivity estimation from sea clutter: An invited review. *Radio Sci.,* **46,** RS6013, doi:10.1029/2011RS004818.

——, ——, ——, ——, and ——, 2012a: Estimation of refractivity using a multiple angle clutter model. *Radio Sci.,* **47,** RS0M07, doi:10.1029/2011RS004701.

——, ——, ——, ——, and ——, 2012b: Multiple grazing angle sea clutter modeling. *IEEE Trans. Antennas Propag.,* **60,** 4408–4417.

Lermusiaux, P., J. Xu, C. F. Chen, S. Jan, L. Y. Chiu, and Y. Yang, 2011: Coupled ocean–acoustic prediction of transmission loss in a continental shelfbreak region: Predictive skill, uncertainty quantification, and dynamical sensitivities. *IEEE J. Oceanic Eng.,* **35,** 895–916.

Liu, W. T., K. B. Katsaros, and J. A. Businger, 1979: Bulk parameterization of air–sea exchanges of heat and water vapor including the molecular constraints at the interface. *J. Atmos. Sci.,* **36,** 1722–1735.

McLay, J. G., C. H. Bishop, and C. A. Reynolds, 2008: Evaluation of the ensemble transform analysis perturbation scheme at NRL. *Mon. Wea. Rev.,* **136,** 1093–1108.

Mentes, S., and Z. Kaymaz, 2007: Investigation of surface duct conditions over Istanbul, Turkey. *J. Appl. Meteor. Climatol.,* **46,** 318–337.

Patterson, W. L., 1998: Advanced Refractive Effects Prediction System (AREPS), version 1.0 user's manual. Space and Naval Warfare System Center Tech. Doc. 3028, 168 pp.

Rogers, L. T., C. P. Hattan, and J. K. Stapleton, 2000: Estimating evaporation duct heights from radar sea echo. *Radio Sci.,* **35,** 955–966, doi:10.1029/1999RS002275.

Rowland, J. R., G. C. Konstanzer, M. R. Neves, R. E. Miller, J. H. Meyer, and J. R. Rottier, 1996: SEAWASP: Refractivity characterization using shipboard sensors. *Proc. 1996 Battlespace Atmospheric Conf.,* San Diego, CA, Naval Command, Control and Ocean Surveillance Center, 155–164.

Skolnik, M. I., 2008: *Radar Handbook*. 3rd ed. McGraw-Hill, 1328 pp.

Thacker, W. C., and O. E. Esenkov, 2002: Assimilating XBT data into HYCOM. *J. Atmos. Oceanic Technol.,* **19,** 709–724.

Thayer, G. D., 1974: An improved equation for the radio refractive index of air. *Radio Sci.,* **9,** 803–807.

Vasudevan, S., R. Anderson, S. Kraut, P. Gerstoft, L. T. Rogers, and J. L. Krolik, 2007: Recursive Bayesian electromagnetic refractivity estimation from radar sea clutter. *Radio Sci.,* **42,** RS2014, doi:10.1029/2005RS003423.

Wang, C., D. Wilson, T. Haack, P. Clark, H. Lean, and R. Marshall, 2012: Effects of initial and boundary conditions of mesoscale models on simulated atmospheric refractivity. *J. Appl. Meteor. Climatol.,* **51,** 115–131.

Warner, T. T., 2011: *Numerical Weather and Climate Prediction*. Cambridge University Press, 526 pp.

Yardim, C., P. Gerstoft, and W. S. Hodgkiss, 2007: Statistical maritime radar duct estimation using a hybrid genetic algorithm—Markov chain Monte Carlo method. *Radio Sci.,* **42,** RS3014, doi:10.1029/2006RS003561.

——, ——, and ——, 2008: Tracking refractivity from clutter using Kalman and particle filters. *IEEE Trans. Antennas Propag.,* **56,** 1058–1070, doi:10.1109/TAP.2008.919205.

——, ——, and ——, 2009: Sensitivity analysis and performance estimation of refractivity from clutter technique. *Radio Sci.,* **44,** RS1008, doi:10.1029/2008RS003897.

Zhao, X., and S. Huang, 2012: Estimation of atmospheric duct structure using radar sea clutter. *J. Atmos. Sci.,* **69,** 2808–2818.